Elongational flow effects on the vortex growth out of Couette flow in ferrofluids

S. Altmeyer[*]

Max Planck Institute for Dynamics and Self-Organization, 37073 Göttingen, Germany

A. Leschhorn

Institut für Grundlagen und Materialien der Elektrotechnik, Universität des Saarlandes, D-66123 Saarbrücken, Germany

Ch. Hoffmann and M. Lücke

Institut für Theoretische Physik, Universität des Saarlandes, D-66123 Saarbrücken, Germany

The growth behavior of stationary axisymmetric vortices and of oscillatory, nonaxisymmetric spiral vortices in Taylor-Couette flow of a ferrofluid in between differentially rotating cylinders is analyzed using a numerical linear stability analysis. The investigation is done as a function of the inner and outer cylinder's rotation rates, the axial wave number of the vortex flows, and the magnitude of an applied homogeneous axial magnetic field. In particular, the consequences of incorporating elongational flow effects in the magnetization balance equation on the marginal control parameters that separate growth from decay behavior are determined. That is done for several values of the transport coefficient that measures the strength of these effects.

I. INTRODUCTION

Ferrofluids [1] as colloidal suspensions of nanosized magnetic particles continue to attract research activities. Some of the reasons are that magnetic fields influence their macroscopic flow behavior and vice versa [1–5] and their rheology and transport properties can be changed by a magnetic field [6–9]. Also, the question of how the flow of a ferrofluid in the Taylor-Couette system is influenced by magnetic fields has been the subject of several theoretical and experimental analyses [10–17], most of them being focused on the relaxation phenomena of the magnetic particles.

It is fair to say that many of these investigations were stimulated by the seminal work of Shliomis and co-workers [9,18,19]. Therein, an expression for the angular velocity of the magnetic particles plays a central role. Because of magnetic torques and dissipation, this velocity differs from the local macroscopic angular velocity $\Omega = \frac{1}{2}(\nabla \times \mathbf{u})$ of the ferrofluid that flows with the macroscopic hydrodynamic velocity field $\mathbf{u}$. The resulting equation for the magnetization field $\mathbf{M}$ of a ferrofluid flowing with velocity $\mathbf{u}$ reduces to a Debye relaxation form [20] if nonlinear terms in $\mathbf{M}$ are ignored.

Thus many authors used in some way a description of ferrofluids that is based on the relaxation of magnetization, which assumes that a ferrofluid can be treated as a system of noninteracting, spherical, magnetically hard particles. However, rheological investigations suggest that ferrofluids can exhibit a significant amount of interparticle interactions that may change their properties. Thus alternatives and extensions of the classical approach [9,18,19] have been sought.

One of these alternatives is the hydrodynamic approach of Müller and Liu [21]. Treating the ferrofluid as a magnetizable continuum, they derived balance equations for the relevant densities and for the spatiotemporal behavior of $\mathbf{M}$ on the basis of the principles of irreversible thermodynamics. Taking

the densities that are conserved in the absence of dissipation, the magnetization, and the electromagnetic field as variables in the thermodynamic energy density, they deduce equations for either the energy or the momentum flux and the entropy production. These equations, together with material-dependent parameters such as susceptibilities and several transport coefficients, provide a full description of the dynamics of ferrofluids. In particular, they find in this way an equation for the time derivative of $\mathbf{M}$.

It contains besides relaxational and flow induced changes [of the well known forms $(\mathbf{u} \cdot \nabla)\mathbf{M}$ and $\Omega \times \mathbf{M}$, respectively] also an additional contribution of the form $\lambda_2 \mathcal{V} \cdot \mathbf{M}$. Here λ_2 is a material-dependent transport coefficient and $\mathcal{V} = \frac{1}{2}[\nabla : \mathbf{u} + (\nabla : \mathbf{u})^T]$ is the symmetric part of the velocity gradient field tensor. Onsager symmetry relations then require [21] that additional forces involving λ_2 appear in the off-equilibrium momentum balance of the ferrofluid.

The material-dependent coefficient λ_2 has to be measured for each ferrofluid separately. From the analysis of an experiment measuring the magnetovortical resonance Müller and Liu inferred a value of $\lambda_2 = 2.54$ [21]. Furthermore, Odenbach and Müller [22] investigated experimentally the nonequilibrium magnetization of a ferrofluid in the Taylor-Couette system subject to a homogeneous transverse magnetic field. They explored the dependence of $\mathbf{M}$ on $\mathcal{V}$ by varying $\mathcal{V}$ in an elongational flow between counterrotating cylinders such that Ω remained constant. Their results reveal that the symmetric velocity gradient field $\mathcal{V}$ can affect the magnetization of a ferrofluid. The authors argued that the magnetization of spherical particles would not be affected by the elongational flow, but that chainlike agglomerates in the fluid that form as a result of interparticle interactions would alter the magnetization dynamics via the term $\lambda_2 \mathcal{V} \cdot \mathbf{M}$. Thus the interparticle interaction of fluids would have an impact on the value of λ_2. For the ferrofluids that they used for their experiments they estimated values of $0 \leqslant \lambda_2 \leqslant 0.88$.

In this paper we investigate the linear growth behavior of stationary axisymmetric and nonaxisymmetric oscillatory

————
[*]sebastian_altmeyer@t-online.de

vortex flow of a ferrofluid in the Taylor-Couette system that is placed in homogeneous axial magnetic fields $\mathbf{H}_{\mathrm{ext}} = H_{\mathrm{ext}}\mathbf{e}_z$. Investigations are done as a function of H_{ext}, the inner and outer cylinder's rotation rates, and the axial wave numbers k of the vortex flows. The marginal parameters that separate growth from decay, i.e., the parameter values for the onset of vortex flow out of the basic homogeneous state of circular Couette flow (CCF), depend sensitively on the presence of any elongational effect, i.e., on the value of the transport coefficient λ_2. Thus we have performed for several values of λ_2 a rather complete linear stability analysis of CCF against the growth of axisymmetry, stationary Taylor vortices [Taylor vortex flow (TVF)] as well as nonaxisymmetric oscillatory spiral vortices [spiral vortex flow (SPI)]. It provides results that can easily be tested by experiments and might contribute to the question of proper magnetization equations and the relevance of the λ_2 term.

II. SYSTEM AND EQUATIONS

A. System

We present numerical results for the growth of vortex perturbations in axially unbounded Taylor-Couette systems with corotating and counterrotating cylinders. The gap width between the outer cylinder of radius r_2 and the inner one of radius r_1 is $d = r_2 - r_1$. With infinitely long cylinders the only relevant parameter characterizing the geometry is the radius ratio $\eta = r_1/r_2$, which is held fixed throughout this paper to $\eta = 0.5$.

The fluid in the annulus is taken to be isothermal and incompressible with kinematic viscosity ν. To characterize the driving of the system, we use the Reynolds numbers

$$\mathrm{Re}_1 = r_1 \Omega_1 d/\nu, \quad \mathrm{Re}_2 = r_2 \Omega_2 d/\nu. \quad (2.1)$$

They just give the reduced azimuthal velocities of the fluid at the inner and outer cylinders, respectively, where Ω_1 and Ω_2 are the respective angular velocities of the cylinders. The inner one is always rotating counterclockwise, so Ω_1 and Re_1 are positive. Further, an external homogeneous axial magnetic field $\mathbf{H}_{\mathrm{ext}} = H_{\mathrm{ext}}\mathbf{e}_z$ is applied.

B. Ferrofluid equations

Here we briefly recapitulate aspects of the more standard form of the ferrofluid equations. Then, in Sec. II C, we show how the latter are modified by the elongational flow terms appearing in the approach of Müller and Liu [21].

The dynamics of the flow of an incompressible ferrofluid is governed by augmented incompressible Navier-Stokes equations. They include magnetic terms that describe the effect of the internal magnetic field $\mathbf{H}$ and the magnetization $\mathbf{M}$ on the balance of momentum density of the ferrofluid resulting in the ferrohydrodynamic equations of motion

$$(\partial_t + \mathbf{u} \cdot \nabla)\mathbf{u} = \nabla^2 \mathbf{u} - \nabla p + 2(\mathbf{M} \cdot \nabla)\mathbf{H} + \nabla \times (\mathbf{M} \times \mathbf{H}),$$
$$\nabla \cdot \mathbf{u} = 0. \quad (2.2)$$

Here we scale lengths by the gap width d, time by the radial momentum diffusion time $\tau_D = d^2/\nu$, velocities with ν/d, and the pressure with $\rho \nu^2/d^2$. The pressure gradient is meant here to contain other terms that can be written as the gradient of

a scalar. The magnetic field $\mathbf{H}$ and the magnetization $\mathbf{M}$ are both reduced by $\sqrt{2\rho/\mu_0}\,\nu/d$, with μ_0 being the permeability and ρ denoting the mass density of the ferrofluid. These two fields are related to each other via the magnetostatic Maxwell equations

$$\nabla \times \mathbf{H} = 0, \quad \nabla \cdot (\mathbf{H} + \mathbf{M}) = 0. \quad (2.3)$$

These equations yield also the relations

$$\mathbf{H}_{\mathrm{out}}(r = r_i) = \mathbf{H}(r = r_i) + M_r(r = r_i)\mathbf{e}_r \quad \text{for} \quad i = 1,2 \quad (2.4)$$

between the internal magnetic field $\mathbf{H}$, the magnetization $\mathbf{M}$, and the magnetic field $\mathbf{H}_{\mathrm{out}}$ outside the ferrofluid, where M_r is the radial component of the magnetization $\mathbf{M}$.

To solve Eqs. (2.2) and (2.3) one additionally needs an equation describing the magnetization dynamics. In the simple Debye approach [20] one considers the relaxation of the magnetization $\mathbf{M}$ towards the equilibrium magnetization

$$\mathbf{M}_{\mathrm{eq}} = \frac{M_{\mathrm{eq}}}{H}\mathbf{H} = \chi(H)\mathbf{H} \quad (2.5)$$

(where M_{eq} and H are the absolute values and χ is the magnetic susceptibility) with one single relaxation time τ in a frame rotating with $\Omega = \frac{1}{2}\nabla \times \mathbf{u}$,

$$(\partial_t + \mathbf{u} \cdot \nabla)\mathbf{M} = -\frac{1}{\tau}(\mathbf{M} - \mathbf{M}_{\mathrm{eq}}) + \Omega \times \mathbf{M}. \quad (2.6)$$

We denote in this paper the combination of Eqs. (2.2) and (2.6) as model D.

C. Elongational flow effects in the Müller-Liu model

1. Magnetization

In the model of Müller and Liu [21] the magnetization dynamics of Eq. (2.6) is augmented by including an additional dependence on the symmetric velocity gradient tensor

$$\mathcal{V} = \tfrac{1}{2}[\nabla : \mathbf{u} + (\nabla : \mathbf{u})^T] \quad (2.7)$$

with a transport coefficient λ_2:

$$(\partial_t + \mathbf{u} \cdot \nabla)\mathbf{M} = -\frac{1}{\tau}(\mathbf{M} - \mathbf{M}_{\mathrm{eq}}) + \Omega \times \mathbf{M} + \lambda_2 \mathcal{V} \cdot \mathbf{M}. \quad (2.8)$$

2. Momentum density

Using our notation, i.e., our scalings given in Sec. II, the equation of [21] for the Cartesian velocity component u_i reads

$$\begin{aligned}(\partial_t + \mathbf{u} \cdot \nabla)u_i = {}& \nabla^2 u_i - \nabla_i p \\ & + 2\nabla_j(H_i B_j) - \nabla_j(M_i h_j - h_i M_j) \\ & + \lambda_2 \nabla_j(M_i h_j + h_i M_j) \end{aligned} \quad (2.9)$$

if one ignores higher-order terms that appear in [21] involving additional transport coefficients λ_3 and λ_4. Here summation over the Cartesian index j is implied and the incompressibility constraint $\nabla_j u_j = 0$ is imposed. Terms that are gradients of scalars are included in Eq. (2.9) in the pressure gradient $\nabla_i p$. Furthermore, $\mathbf{B} = \mathbf{H} + \mathbf{M}$ and $\mathbf{h} = \mathbf{H}_{\mathrm{eq}} - \mathbf{H}$, with $\mathbf{H}_{\mathrm{eq}}(\mathbf{M})$ being the inverse function of $\mathbf{M}_{\mathrm{eq}}(\mathbf{H})$.

To compare Eq. (2.9) with the momentum balance equation (2.2) one first notes that

$$2\nabla_j(H_i B_j) = 2(\mathbf{M} \cdot \nabla)H_i + \nabla_i(\mathbf{H} \cdot \mathbf{H}). \quad (2.10)$$

Here Maxwell's equation $\nabla \cdot (\mathbf{M} + \mathbf{H}) = 0$ has been used. The gradient of $\mathbf{H} \cdot \mathbf{H}$ in Eq. (2.10) can be incorporated into the pressure gradient of Eq. (2.9). Second, one has

$$-\nabla_j(M_i h_j - h_i M_j) = [\nabla \times (\mathbf{M} \times \mathbf{H})]_i \qquad (2.11)$$

since $\mathbf{H}_{\mathrm{eq}}$ is parallel to $\mathbf{M}$. Thus the Müller-Liu (ML) momentum balance equation (2.9) agrees with (2.2), except that the former contains an additional forcing term involving the coefficient λ_2 that is related to the elongational effect in the magnetization equation (2.8).

For later use we rewrite this additional forcing term in Eq. (2.9) using the equality

$$\nabla_j(M_i h_j + h_i M_j) = M_i(\nabla \cdot \mathbf{h}) + h_i(\nabla \cdot \mathbf{M})$$
$$- [\mathbf{h} \times (\nabla \times \mathbf{M})]_i + \nabla_i(\mathbf{h} \cdot \mathbf{M}). \qquad (2.12)$$

The last contribution in the above equation being the gradient of $\mathbf{h} \cdot \mathbf{M}$ can be incorporated into the pressure gradient term.

Thus the ML momentum balance equation (2.9) for an incompressible ferrofluid can be written in the form

$$\nabla \cdot \mathbf{u} = 0, \qquad (2.13a)$$
$$(\partial_t + \mathbf{u} \cdot \nabla)\mathbf{u} = \nabla^2\mathbf{u} - \nabla p + 2(\mathbf{M} \cdot \nabla)\mathbf{H} + \nabla \times (\mathbf{M} \times \mathbf{H})$$
$$+ \lambda_2[\mathbf{M}(\nabla \cdot \mathbf{h}) + \mathbf{h}(\nabla \cdot \mathbf{M}) - \mathbf{h} \times (\nabla \times \mathbf{M})],$$
$$(2.13b)$$

which we will use in the following. Note that the additional forcing of the flow by the λ_2 term is linear in the deviation $\mathbf{h}$ of the magnetic field $\mathbf{H}$ from the equilibrium field $\mathbf{H}_{\mathrm{eq}}$.

In the remainder of this paper we denote the combination of Eqs. (2.8) and (2.13) as model ML. Furthermore, we would like to mention that model ML reduces for vanishing transport coefficient $\lambda_2 = 0$ to model D.

III. LINEAR STABILITY ANALYSIS OF CIRCULAR COUETTE FLOW

In this section and the Appendix we present the mathematical tools for the linear stability analysis of the basic CCF state.

A. Basic state: Circular Couette flow

The velocity field of CCF solves the ferrohydrodynamic equations of motion (2.2) and (2.13) also when a homogeneous axial field $\mathbf{H}_{\mathrm{ext}} = H_{\mathrm{ext}}\mathbf{e}_z$ is applied. Then the homogeneous internal field $\mathbf{H}_{\mathrm{CCF}}$ and the equilibrium magnetization $\mathbf{M}_{\mathrm{CCF}}$,

$$\mathbf{H}_{\mathrm{CCF}} = \mathbf{H}_{\mathrm{ext}} = \mathbf{H}_{\mathrm{eq}},$$
$$\mathbf{M}_{\mathrm{CCF}} = \mathbf{M}_{\mathrm{eq}}(\mathbf{H}_{\mathrm{CCF}}) = \chi(H_{\mathrm{ext}})\mathbf{H}_{\mathrm{ext}}, \qquad (3.1)$$

fulfill the Maxwell equations (2.3) and the boundary conditions (2.4). In this case, the magnetic terms in the equations of motion (2.2) and (2.13) vanish. Note that $\mathbf{H}_{\mathrm{CCF}} = \mathbf{H}_{\mathrm{eq}}(\mathbf{M}_{\mathrm{CCF}}) = H_{\mathrm{ext}}\mathbf{e}_z$, so $\mathbf{h}_{\mathrm{CCF}} = 0$.

Thus the basic CCF velocity field

$$\mathbf{u}_{\mathrm{CCF}} = (A_{\mathrm{CCF}}r + B_{\mathrm{CCF}}r^{-1})\mathbf{e}_\varphi \qquad (3.2)$$

solves the ferrohydrodynamic equations of motion (2.2) and (2.13). The here assumed no-slip boundary conditions

$$\mathbf{u}(r = r_1) = \mathrm{Re}_1\mathbf{e}_\varphi, \quad \mathbf{u}(r = r_2) = \mathrm{Re}_2\mathbf{e}_\varphi \qquad (3.3)$$

yield the coefficients $A_{\mathrm{CCF}} = (\mathrm{Re}_2 - \eta\mathrm{Re}_1)/(1 + \eta)$ and $B_{\mathrm{CCF}} = \eta(\mathrm{Re}_1 - \eta\mathrm{Re}_2)/(1 + \eta)(1 - \eta)^2$.

In this CCF state, the vorticity and the velocity gradient tensor read

$$\Omega_{\mathrm{CCF}} = A_{\mathrm{CCF}}\mathbf{e}_z, \quad \mathcal{V}_{\mathrm{CCF}} = -\frac{B_{\mathrm{CCF}}}{r^2}(\mathbf{e}_r : \mathbf{e}_\varphi + \mathbf{e}_\varphi : \mathbf{e}_r). \quad (3.4)$$

The magnetization equations (2.6) and (2.8) are fulfilled because $\mathbf{M}_{\mathrm{CCF}}$ is parallel to $\mathbf{e}_z$ and $\Omega_{\mathrm{CCF}} \times \mathbf{e}_z = 0 = \mathcal{V}_{\mathrm{CCF}} \cdot \mathbf{e}_z$.

B. Linearization around the CCF state

In the following $\mathbf{u}, p, \mathcal{V}, \Omega$ and $\delta\mathbf{H}, \delta\mathbf{M}, \delta\mathbf{h} = \mathbf{h}$ denote deviations from the CCF state. Then the ferrofluid equations of model ML read after linearization around the CCF state

$$0 = \nabla \cdot \mathbf{u}, \qquad (3.5a)$$
$$\partial_t\mathbf{u} = -(\mathbf{u}_{\mathrm{CCF}} \cdot \nabla)\mathbf{u} - (\mathbf{u} \cdot \nabla)\mathbf{u}_{\mathrm{CCF}} + \nabla^2\mathbf{u} - \nabla p$$
$$- \mathbf{M}_{\mathrm{CCF}}(\nabla \cdot \delta\mathbf{M}) + \nabla \times (\delta\mathbf{M} \times \mathbf{H}_{\mathrm{CCF}})$$
$$+ \lambda_2\mathbf{M}_{\mathrm{CCF}}(\nabla \cdot \mathbf{h}), \qquad (3.5b)$$
$$\partial_t\delta\mathbf{M} = -(\mathbf{u}_{\mathrm{CCF}} \cdot \nabla)\delta\mathbf{M} - \frac{1}{\tau}(\delta\mathbf{M} - \delta\mathbf{M}_{\mathrm{eq}}) + \Omega_{\mathrm{CCF}} \times \delta\mathbf{M}$$
$$+ \Omega \times \mathbf{M}_{\mathrm{CCF}} + \lambda_2(\mathcal{V} \cdot \mathbf{M}_{\mathrm{CCF}} + \mathcal{V}_{\mathrm{CCF}} \cdot \delta\mathbf{M}). \quad (3.5c)$$

Here we have used Maxwell's equations (2.3) to eliminate $\delta\mathbf{H}$ in favor of $\delta\mathbf{M}$. Furthermore, we have incorporated terms that can be written as gradients of a scalar into the pressure gradient like the ones that appear in the contributions $2(\mathbf{M}_{\mathrm{CCF}} \cdot \nabla)\delta\mathbf{H} = 2\nabla(\mathbf{M}_{\mathrm{CCF}} \cdot \delta\mathbf{H})$ and $\nabla \times (\mathbf{M}_{\mathrm{CCF}} \times \delta\mathbf{H}) = -\nabla(\mathbf{M}_{\mathrm{CCF}} \cdot \delta\mathbf{H}) - \mathbf{M}_{\mathrm{CCF}}(\nabla \cdot \delta\mathbf{M})$.

Into the linearized ferrofluid equation (3.5c) enters the equilibrium magnetization function for the perturbed internal magnetic field $\mathbf{H}_{\mathrm{CCF}} + \delta\mathbf{H}$ via its deviation from the one characterizing the CCF state

$$\delta\mathbf{M}_{\mathrm{eq}} = \mathbf{M}_{\mathrm{eq}}(\mathbf{H}_{\mathrm{CCF}} + \delta\mathbf{H}) - \mathbf{M}_{\mathrm{eq}}(\mathbf{H}_{\mathrm{CCF}}). \qquad (3.6)$$

It enters also into the momentum balance equation (3.5b) via the last term since $\nabla \cdot \mathbf{h} = \nabla \cdot (\mathbf{H}_{\mathrm{eq}} - \mathbf{H}) = \nabla \cdot (\mathbf{M} - \mathbf{M}_{\mathrm{eq}}) = \nabla \cdot (\delta\mathbf{M} - \delta\mathbf{M}_{\mathrm{eq}})$ according to Maxwell's equations (2.3). In solving Eqs. (3.5) we have ignored, as in Ref. [16], the deviation of $\delta\mathbf{M}_{\mathrm{eq}}$ relative to the direct magnetization perturbation $\delta\mathbf{M}$. We expect also here the contribution of the former to be small compared to the latter.

The equations (3.5) with $\delta\mathbf{M}_{\mathrm{eq}} = 0$ are presented in the Appendix using cylindrical coordinates with $\mathbf{u} = u\mathbf{e}_r + v\mathbf{e}_\varphi + w\mathbf{e}_z$ and $\delta\mathbf{M} = \delta M_r\mathbf{e}_r + \delta M_\varphi\mathbf{e}_\varphi + \delta M_z\mathbf{e}_z$. They are solved with the ansatz

$$(u, v, w, p, \delta M_r, \delta M_\varphi, \delta M_z)$$
$$= e^{\sigma t + im\varphi + ikz}(U, V, W, P, \hat{M}_r, \hat{M}_\varphi, \hat{M}_z) \qquad (3.7)$$

for vortex perturbations. Here k is the axial wave number of the vortex mode and m the azimuthal one. The real part γ of the complex eigenvalue $\sigma = \gamma + i\omega$ gives the temporal growth rate of the k-m mode and the imaginary part ω its oscillation frequency. The mode amplitudes $U, V, W, P, \hat{M}_r, \hat{M}_\varphi, \hat{M}_z$ depend on the radial coordinate r.

We have solved the ordinary differential equations for the mode amplitudes with a standard shooting method [23,24] as described in detail in the Appendix. In this way we determine at different fixed values of $\mathrm{Re}_2, m, k, H_{\mathrm{ext}}$, and λ_2 the marginal

values of Re_1 and ω for which vortex perturbations show zero growth, $\gamma = 0$. We would like to note that we use in the remainder of this paper the letter H without a subscript to represent H_{ext} for the sake of notational simplicity.

IV. RESULTS AND DISCUSSION

In this section we present our results for the λ_2 dependence of the stability boundaries of the CCF state against vortex perturbations. Since these boundaries are the bifurcation thresholds for the respective nonlinear vortex states we will use the terms "stability boundary," "bifurcation threshold," and "onset of vortex flow" interchangeably.

We restrict ourselves in this work to $m = 0$ Taylor vortices and spiral vortex perturbations with azimuthal wave number $m = \pm 1$. For the latter also the λ_2 dependence of the marginal spiral frequencies at onset is determined. Note that the axial magnetic fields considered here do not break the axial mirror symmetry between left and right handed spiral vortices. So it suffices to present the results for $m = 1$ vortex perturbations (the mirror-symmetric ones for $m = -1$ spirals are meant to be included as well). Furthermore, a few test calculations showed that the results for vortex perturbations with azimuthal wave number $m > 1$ are qualitatively similar.

A. Ferrofluid parameters

For our calculations we use typical values of the parameters [25–28] that characterize the ferrofluid APG933 of FerroTec: $M_{\text{mat}}^{\text{sat}} \simeq 450\,\text{kA/m}$, $\Phi = 4.1\%$, $\rho\nu = 0.5\,\text{Pa s}$, $s = 2\,\text{nm}$, $f_0 = 10^9\,\text{Hz}$, and $K = 15\,\text{kJ/m}^3$. The equilibrium magnetization $M_{\text{eq}}(H)$ of APG933 is obtained with a polydisperse fit to experimental data that is described in detail in Ref. [16]. For the single magnetic relaxation time τ we use a value of 0.5×10^{-3} s, which is comparable to the averaged effective relaxation time as well as experimental results [29,30].

We consider in this work the range $0 \leqslant \lambda_2 \leqslant 0.8$ for the coefficient λ_2, thereby orienting ourselves at the experimental results of Ref. [22]. Note, however, that the transport coefficient can be expected to depend on the properties of the particular ferrofluid [21].

For better comparison with experimental results, in this section we use the physical units kA/m for the magnetic field.

B. Stability boundaries in the Re_2-Re_1 plane

We first discuss here how the parameter λ_2 influences the growth of $m = 0$ and $m = 1$ vortex perturbations out of the CCF state in the Re_2-Re_1 plane of Reynolds numbers. To that end we determine the stability of the CCF state against these perturbations.

Figure 1 presents the bifurcation thresholds for axisymmetric $m = 0$ and nonaxisymmetric $m = 1$ vortex flow in a magnetic field $H = 67.7\,\text{kA/m}$ resulting from model ML. As a representative axial wave number we have chosen in Fig. 1 $k = 2.8274$ as in experiments [31]. Figure 1(c) shows the spiral frequencies at the bifurcation thresholds of Fig. 1(b) that are to be discussed later on in Sec. IV D.

The lowest thick solid curve in each plot refers to the case without any magnetic field $H = 0$. Thus the CCF basic state is stabilized against the two types of vortex perturbations in the
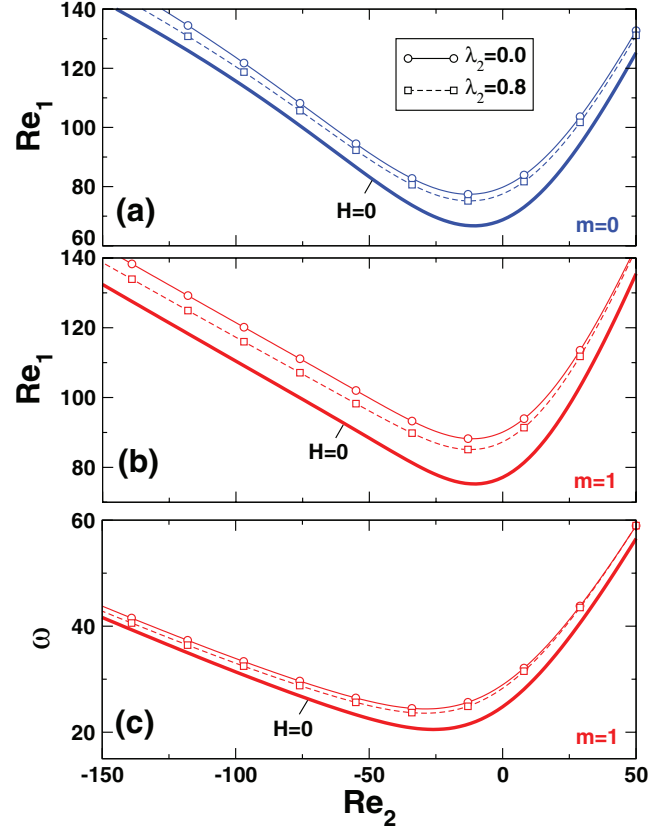

FIG. 1. (Color online) Stability thresholds of the CCF state against growth of (a) $m = 0$ TVF and (b) $m = 1$ SPI in the Re_2-Re_1 plane of control parameters. (c) SPI frequencies at the bifurcation thresholds of (b). Thin solid and dashed lines with symbols show the results of model ML for $\lambda_2 = 0$ and $\lambda_2 = 0.8$ for a magnetic field $H = 67.7$ kA/m. The lowest thick curve refers in each figure to the absence of a magnetic field $\mathbf{H} = 0$. The axial wave number is $k = 2.8274$.

magnetic field. This behavior has been seen already [15,16,31] for $\lambda_2 = 0$. Here we want to remind the reader that for $\lambda_2 = 0$ model ML reduces to model D.

Taking into account λ_2, the basic state becomes destabilized in comparison with the case $\lambda_2 = 0$: The bifurcation thresholds of both $m = 0$ and $m = 1$ vortices are shifted again to lower values of Re_1. Thus, for the axial wave number of $k = 2.8274$ used in Fig. 1, the λ_2 term reduces the general stabilization effect caused by a magnetic field. Such a λ_2-induced relative destabilization is predicted by model ML in the whole range of Re_2 shown in Fig. 1. However, the changes of the stability boundaries that are induced by λ_2 are quite weak, in particular for corotating cylinders.

Comparing Figs. 1(a) and 1(b), one observes that the $\lambda_2 = 0$ bifurcation thresholds for nonaxisymmetric $m = 1$ vortex flow are modified more by the magnetic field than those for $m = 0$ Taylor vortices. The upward shift towards larger values of Re_1 of the former is larger than for the latter. This effect has been found to show up also in transversal and oblique magnetic fields [15,31].

Also the magnitude of the modifications caused by a finite λ_2 is larger for $m = 1$ than for $m = 0$ perturbations. Thus the field-induced stabilization against the growth of $m = 1$
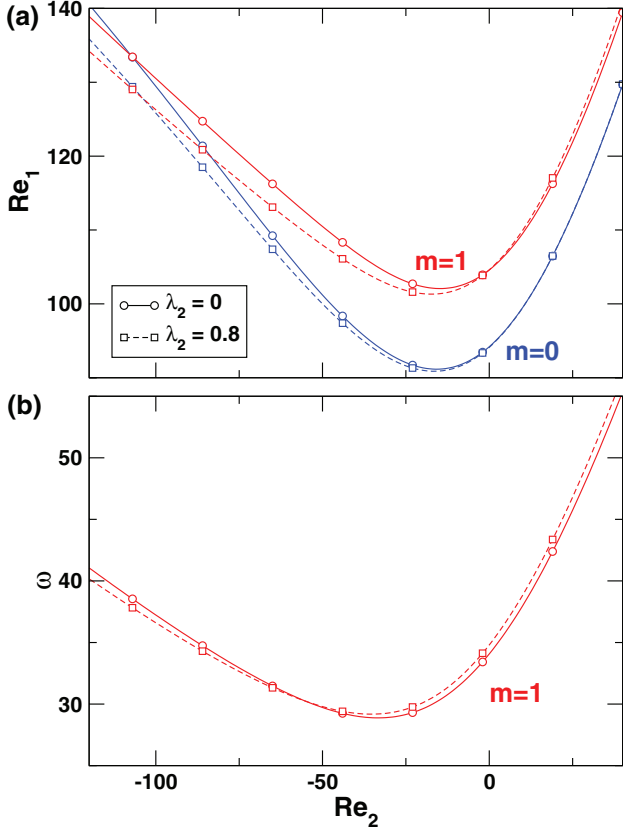
FIG. 2. (Color online) Influence of the elongational flow effect on marginal vortex perturbations with a larger wave number $k = 3.4558$. Shown are (a) bifurcation thresholds of $m = 0$ TVF and $m = 1$ SPI and (b) the spiral frequencies at threshold versus Re_2. Solid and dashed lines refer to $\lambda_2 = 0$ and 0.8, respectively. The magnetic field is $H = 135.4$ kA/m.

vortices gets for $k = 2.8274$ reduced more by the adverse effect of λ_2, but not deleted.

We would like to stress that, in contrast to the stabilization of the CCF state by a magnetic field, the λ_2-induced modifications of the linear growth of vortices do depend significantly on their axial wave number, as will be shown in more detail in Sec. IV E.

Here we first discuss the situation for a larger wave number, taking $k = 3.4558$ as a representative example. This situation is more complex than the one shown in Fig. 1 for vortices with the smaller wave number $k = 2.8274$. Incorporating the flow elongation for the latter by λ_2 increases their growth rate and thus shifts the stability boundaries in Fig. 1 downward for all Re_2 shown there. Figure 2, in contrast, shows that vortex perturbations with the larger wave number $k = 3.4558$ experience for finite λ_2 an increased growth for strong negative Re_2, but a reduced growth in the corotating case: In Fig. 2(a) the bifurcation thresholds of TVF ($m = 0$) and in particular of SPI ($m = 1$) are shifted downward for strongly counterrotating cylinders, but slightly upward for corotating ones when the elongational term is switched on.

C. Stability boundaries: *H* dependence

Figure 3 shows how the bifurcation thresholds of model ML for $m = 0$ TVF and for $m = 1$ SPI vary with the magnetic
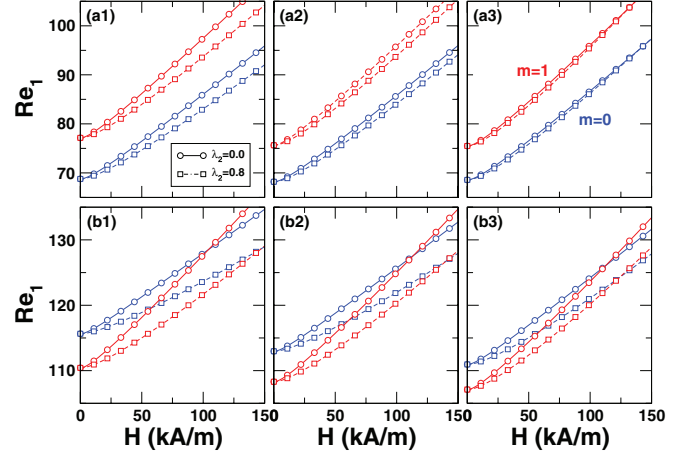

FIG. 3. (Color online) Variation of the $m = 0$ and $m = 1$ bifurcation thresholds with magnetic field H resulting from model ML for $\lambda_2 = 0$ (lines with circles) and $\lambda_2 = 0.8$ (lines with squares). The top row refers to $Re_2 = 0$ and the bottom one to $Re_2 = -100$. The wave numbers are, from left to right, $k = 2.8274$, 3.1415, and 3.4558.

field and how this variation is influenced by incorporating the elongational flow effect. The top row of figures refers to $Re_2 = 0$ and the bottom one to $Re_2 = -100$. The wave numbers are $k = 2.8274$, 3.1415, and 3.4558 from left to right.

Except for small H, all thresholds increase linearly with H with slopes $\partial Re_{1,\text{stab}}(H)/\partial H$ that vary slightly with λ_2 and with wave number k. For $Re_2 = 0$ in Figs. 3(a1)–3(a3) the slopes of the $m = 0$ and $m = 1$ curves are comparable; however, they differ significantly for counterrotating cylinders, e.g., $Re_2 = -100$ in Figs. 3(b1)–3(b3). Consequently, there are intersections of the $m = 0$ and $m = 1$ stability boundaries, an effect that has been seen also in experiments and also in full nonlinear simulations [15] with $\lambda_2 = 0$.

Figure 3 shows that the modifications of the H dependence of the bifurcation thresholds due to λ_2 tend to increase when the outer cylinder Reynolds number Re_2 becomes more negative, i.e., when the strain increases. Furthermore, they depend on the axial wave number k (see also Sec. IV E). Here, in Fig. 3 one observes that for fixed k the modifications due to λ_2 increase with increasing magnetic field while remaining qualitatively the same. The general tendency to be seen in Fig. 3 is that the elongational effect shifts the stability boundaries downward in Re_1 by amounts that depend on k and Re_2. Thus the stabilization by the magnetic field being significantly larger overcompensates for the small adverse destabilizing elongational effect.

D. Spiral frequencies

So far we have discussed in Secs. IV B and IV C the influence of the elongational term on the growth rates of $m = 0$ and $m = 1$ vortex perturbations, i.e., on the real part of the eigenvalue of these solutions via the location of the corresponding bifurcation thresholds in parameter space. Here we discuss our results on the imaginary part of the marginal eigenvalue at the bifurcation threshold of $m = 1$ vortex flow, i.e., on the marginal spiral frequency ω.
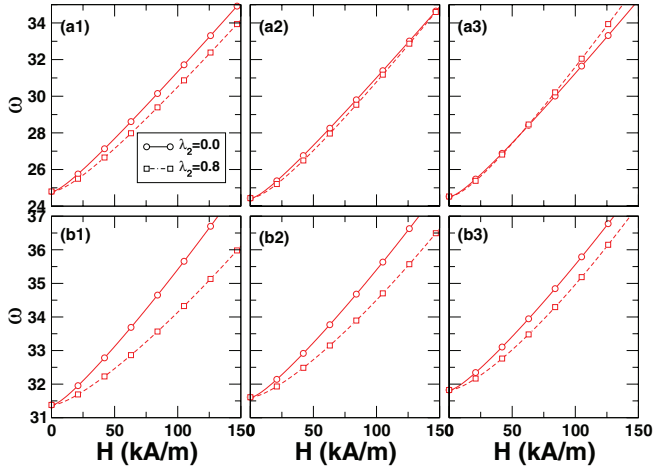
FIG. 4. (Color online) Same as in Fig. 3, but for frequencies ω of $m = 1$ spirals at the bifurcation thresholds.

To that end we present in Fig. 4 the SPI frequencies at the $m = 1$ bifurcation thresholds of Fig. 3 versus magnetic field H. The selected values of λ_2, k, and Re_2 and the presentation mode are the same as in Fig. 3.

First, as the main effect one has to note that the SPI frequencies increase with the field H simply because the onset Reynolds numbers Re_1 in Fig. 3 increase with H. For the same reason the frequencies are larger for $Re = -100$ than for $Re = 0$. A secondary and minor effect comes from switching on the elongational term. It typically shifts the onset downward to slightly smaller values of Re_1 and thus the SPI frequency ω shows a similar, small, λ_2-induced reduction. The magnitude of the latter depends on H, k, and Re_2. Note, however, that the elongational effect causes for the larger wave number in Fig. 4 at $Re = 0$ a slight increase of ω, in particular for larger H. Strong counterrotating cylinders, in contrast, reduce in general the frequency for finite λ_2 as shown in the bottom row of Fig. 4.

The modifications of the spiral frequencies due to finite λ_2 are most pronounced for the lowest wave number $k = 2.8274$ in counterrotating cylinders [see Fig. 4(b1)]. In all cases, switching on the elongational term does not cause dramatic changes in the field dependence of the SPI frequencies. All in all, the behavior of the imaginary part of the marginal eigenvalue with increasing λ_2 is quite similar to that of its real part.

E. Wave number dependence of stability boundaries and spiral frequencies

So far we have investigated the influence of the elongational effect on the eigenvalues for vortex growth out of the CCF state for a few fixed axial wave numbers k. Here we discuss in more detail how the λ_2 term changes the wave number dependence of the stability boundaries and of the spiral frequencies. This is of interest also with respect to experiments since the wave numbers of some vortex structures show a strong variation when changing the magnetic field [31,32]. Furthermore, also hysteresis [31] between vortex flows with different k has been observed when increasing and decreasing the Reynolds numbers.
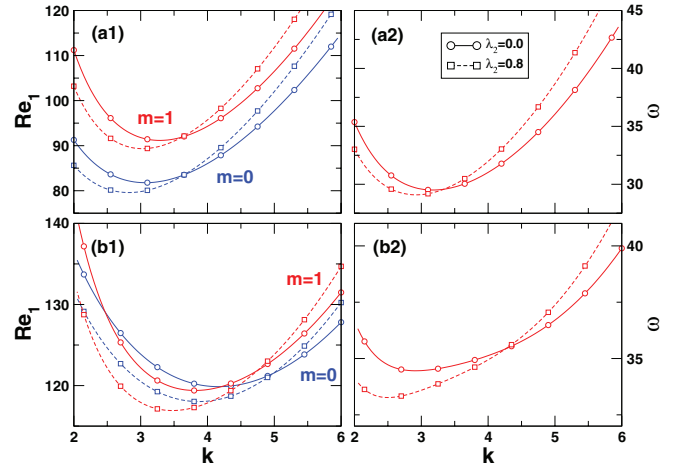

FIG. 5. (Color online) The left column shows the stability boundaries of the CCF state against the growth of $m = 0$ and $m = 1$ vortex flow in the k-Re_1 plane for $\lambda_2 = 0$ and 0.8. The right column shows the marginal spiral frequencies at the $m = 1$ thresholds that are displayed in the left column. The top row refers to $Re_2 = 0$ and the bottom one to $Re_2 = -100$. The magnetic field is $H = 80\,\text{kA/m}$.

The left column of Fig. 5 shows how the bifurcation thresholds for $m = 0$ and $m = 1$ vortex flow in the k-Re_1 plane change when the elongational term is incorporated in the ferrofluid equations (2.8) and (2.13) of model ML. The right column of Fig. 5 shows the wave number dependence of the corresponding marginal spiral frequencies at the onsets that are are displayed in the left column. The top row refers to $Re_2 = 0$ and the bottom one to $Re_2 = -100$. The magnetic field is fixed at $H = 80\,\text{kA/m}$.

One sees that, relative to the $\lambda_2 = 0$ results, the thresholds for the case of $\lambda_2 = 0.8$ (lines with squares) are shifted downward in Re_1 at smaller k and upward at larger wave numbers. Thus, in a fixed magnetic field the elongational effect destabilizes (stabilizes) the CCF state against growth of vortices when their wave numbers are small (large). This qualitative observation holds for all thresholds that are shown in Fig. 5. Thus model ML predicts a crossing of the pair of respective stability curves for $\lambda_2 = 0$ and 0.8 at a specific value $k_\times$ of the wave number: Increasing λ_2 destabilizes the basic CCF state against perturbations with small wave numbers, while stabilization occurs for larger k. This holds for $m = 0$ and $m = 1$ perturbations.

For TVF [31,32] the typical experimentally observed wave numbers lie around $k \approx 3$, e.g., $k = 2.51$, 2.83, and 3.14. For all these wave numbers, model ML predicts the basic state to become destabilized by a finite λ_2 compared to the case without it.

In Fig. 5(a1) one sees that the crossover values of $k_\times$ for $m = 0$ and $m = 1$ perturbations are almost identical when the outer Reynolds number is zero. Additional simulations for various different parameters have shown that this coincidence of $k_\times$ for $m = 0$ and $m = 1$ vortices is special for $Re_2 \approx 0$.

Also the spiral frequencies in the right column of Fig. 5 increase with increasing λ_2 when k is large, but decrease for smaller k as a result of switching on the elongational effect. However, the crossing wave number that separates the ω increase from the ω decrease is slightly smaller than the

crossing location $k_\times$ of the $m = 1$ stability thresholds. An analysis of experimental vortex flows with wave numbers that are larger and smaller than $k_\times$ and the comparison with the predictions of the model for the bifurcation thresholds and spiral frequencies could help to show whether the elongational effect is at work and how large λ_2 might be.

A reasonable looking kind of hand waving explanation for the wave number dependence of the λ_2 effect on the growth rates of vortex flow might be given if one follows a speculation [22] on the physical origin of the elongational effect. In Ref. [22] Odenbach and Müller argue that the microscopic origin of a finite λ_2 might be attributed to the finite asphericity of the colloids, i.e., the presence of (short) particle chains in the ferrofluid. These chains could more easily remain aligned in the direction of the magnetic field in vortex flows with small k than in a flow with large axial wave number and large azimuthal vorticity. Thus, since the magnetorotational dissipation in the latter flow is larger than in the former one it requires larger centrifugal forces, i.e., larger values of Re_1, to drive the growth of a large k flow. The weakness of this argumentation is, however, that one would expect in the presence of chains also for small k vortices an increase of the threshold Reynolds number. In contrast, model ML predicts that incorporating the elongational term in the magnetization balance changes the momentum balance of the vortex flow such that the growth of vortices is enhanced for $k < k_\times$ and reduced for $k > k_\times$ relative to the reference case of $\lambda_2 = 0$.

V. CONCLUSION

The consequences of incorporating elongational flow effects in the magnetization balance of ferrofluids on the growth behavior of vortex flow in the Taylor-Couette system were investigated. Orienting ourselves at experimental estimations for the magnitude of the elongational effect [22], we explored values of the transport coefficient λ_2 that measures its strength between 0 and 0.8. Model ML was used to do a linear analysis of the dynamics of the vortex perturbations of the CCF state in the presence of an axial magnetic field. Here we considered in detail stationary $m = 0$ axisymmetric Taylor vortex perturbations and oscillatory nonaxisymmetric $m = 1$ spiral vortex flow.

In general, magnetic fields stabilize the basic CCF state against vortex growth; however, when taking λ_2 into account we found modifications of this stabilization. Depending on, e.g., the outer cylinder's Reynolds number Re_2 and the axial wave number k of the vortex flow the primary, field induced stabilization can be either enhanced or reduced by

the elongational flow induced contributions in the ferrofluid equations of model ML. Thus, in the presence of a magnetic field, the growth rates for vortex flow can be either reduced or enhanced, respectively, relative to the $\lambda_2 = 0$ reference situation. However, in any case, i.e., for all parameter configurations that we have explored, the elongational effect was never big enough to overcompensate for the general, field induced stabilization; only the magnitude of the latter was modified by taking into account a finite λ_2.

These modifications are typically larger for nonaxisymmetric $m = 1$ spiral vortices than for axisymmetric $m = 0$ Taylor vortices, but their variations with Re_2 and k are qualitatively similar. Furthermore, for $m = 0$ as well as for $m = 1$ vortices, the λ_2 terms cause a significant relative growth enhancement of vortex flow with small k but a growth reduction when k is larger.

The λ_2-induced modifications of the spiral frequencies ω at onset of vortex flow, i.e., of the imaginary parts of the marginal eigenvalues, follow largely the changes of the bifurcation thresholds for spiral flow. When a finite λ_2 shifts the latter upward (downward) in Reynolds number Re_1 the marginal spiral frequency increases (decreases) accordingly as a consequence of the close relation between the spiral's rotation rate and that of the inner cylinder. Thus also the marginal spiral frequencies show with increasing λ_2 an upward shift for large k and a downward shift for small k.

Given that the Taylor-Couette system provides very good conditions for well controlled experiments on the behavior of vortices, we hope that our results generate enough interest to address the question of the relevance of any elongational effect also experimentally. Its marked wave number dependence and its influence on the spiral frequencies might possibly be large enough to obtain experimental information on the magnitude of λ_2 in comparison with the model results presented here.

APPENDIX: SOLVING THE LINEARIZED EQUATIONS (3.5)

Here we give more details on the way we solved Eqs. (3.5) using cylindrical coordinates. For the sake of notational simplicity we use in this appendix the symbol H to represent H_{ext}.

The linearized equations (3.5) of model ML for $\mathbf{u} = u\mathbf{e}_r + v\mathbf{e}_\varphi + w\mathbf{e}_z$ and $\delta\mathbf{M} = \delta M_r\mathbf{e}_r + \delta M_\varphi\mathbf{e}_\varphi + \delta M_z\mathbf{e}_z$ read in cylindrical coordinates

$$0 = \left(\partial_r + \frac{1}{r}\right)u + \frac{1}{r}\partial_\varphi v + \partial_z w, \tag{A1}$$

$$\partial_t u = -\frac{v_{\text{CCF}}}{r}\partial_\varphi u + \frac{2v_{\text{CCF}}}{r}v - \partial_r p + \frac{1}{r}\partial_\varphi\left[\frac{1}{r}\partial_\varphi u - \left(\partial_r + \frac{1}{r}\right)v\right] + \partial_z(\partial_z u - \partial_r w) + H\partial_z\delta M_r, \tag{A2}$$

$$\partial_t v = -2A_{\text{CCF}}u - \frac{v_{\text{CCF}}}{r}\partial_\varphi v - \frac{1}{r}\partial_\varphi p + \partial_r\left[\left(\partial_r + \frac{1}{r}\right)v - \frac{1}{r}\partial_\varphi u\right] + \partial_z\left(\partial_z v - \frac{1}{r}\partial_\varphi w\right) + H\partial_z\delta M_\varphi, \tag{A3}$$

$$\partial_t w = -\frac{v_{\mathrm{CCF}}}{r}\partial_\varphi w - \partial_z p - \left(\partial_r + \frac{1}{r}\right)(\partial_z u - \partial_r w) - \frac{1}{r}\partial_\varphi\left(\partial_z v - \frac{1}{r}\partial_\varphi w\right) - H\left[\left(\partial_r + \frac{1}{r}\right)\delta M_r + \frac{1}{r}\partial_\varphi \delta M_\varphi\right]$$

$$- (1-\lambda_2)\chi H\left[\left(\partial_r + \frac{1}{r}\right)\delta M_r + \frac{1}{r}\partial_\varphi \delta M_\varphi + \partial_z \delta M_z\right], \tag{A4}$$

$$\partial_t \delta M_r = -\frac{1}{\tau}\delta M_r - \frac{v_{\mathrm{CCF}}}{2}\frac{1}{r}\partial_\varphi \delta M_r + (1-\lambda_2)\frac{B_{\mathrm{CCF}}}{r^2}\delta M_\varphi - \frac{v_{\mathrm{CCF}}}{2}\frac{1}{r}\partial_\varphi \delta M_z + \frac{1}{2}\chi H[\partial_z u - \partial_r w + \lambda_2(\partial_z u + \partial_r w)], \tag{A5}$$

$$\partial_t \delta M_\varphi = -\frac{1}{\tau}\delta M_\varphi - (1+\lambda_2)\frac{B_{\mathrm{CCF}}}{r^2}\delta M_r - v_{\mathrm{CCF}}\frac{1}{r}\partial_\varphi \delta M_\varphi + \frac{1}{2}\chi H\left[\partial_z v - \frac{1}{r}\partial_\varphi w + \lambda_2\left(\partial_z v + \frac{1}{r}\partial_\varphi w\right)\right], \tag{A6}$$

$$\partial_t \delta M_z = -\frac{1}{\tau}\delta M_z - v_{\mathrm{CCF}}\frac{1}{r}\partial_\varphi \delta M_z + \lambda_2 \chi H \partial_z w. \tag{A7}$$

Inserting the solution ansatz (3.7) for the vortex perturbation fields with the temporal eigenvalue $\sigma = \gamma + i\omega$ yields the set of ordinary differential equations for the amplitudes of the m-k mode

$$0 = \left(\partial_r + \frac{1}{r}\right)U + \frac{im}{r}V + ikW, \tag{A8}$$

$$\sigma U = -v_{\mathrm{CCF}}\frac{im}{r}U + \frac{2v_{\mathrm{CCF}}}{r}V - \partial_r P + \frac{im}{r}\left[\frac{im}{r}U - \left(\partial_r + \frac{1}{r}\right)V\right] + ik(ikU - \partial_r W) + ikH\hat{M}_r, \tag{A9}$$

$$\sigma V = -2A_{\mathrm{CCF}}U - v_{\mathrm{CCF}}\frac{im}{r}V - \frac{im}{r}P + \partial_r\left[\left(\partial_r + \frac{1}{r}\right)V - \frac{im}{r}U\right] + ik\left(ikV - \frac{im}{r}W\right) + ikH\hat{M}_\varphi, \tag{A10}$$

$$\sigma W = -v_{\mathrm{CCF}}\frac{im}{r}W - ikP + \left(\partial_r + \frac{1}{r}\right)(\partial_r W - ikU) - \frac{im}{r}\left(ikV - \frac{im}{r}W\right) - H\left[\left(\partial_r + \frac{1}{r}\right)\hat{M}_r + \frac{im}{r}\hat{M}_\varphi\right]$$

$$- (1-\lambda_2)\chi H\left[\left(\partial_r + \frac{1}{r}\right)\hat{M}_r + \frac{im}{r}\hat{M}_\varphi + ik\hat{M}_z\right], \tag{A11}$$

$$\sigma \hat{M}_r = -\frac{1}{\tau}\hat{M}_r - \frac{v_{\mathrm{CCF}}}{2}\frac{im}{r}\hat{M}_r + (1-\lambda_2)\frac{B_{\mathrm{CCF}}}{r^2}\hat{M}_\varphi - \frac{v_{\mathrm{CCF}}}{2}\frac{im}{r}\hat{M}_z + \frac{1}{2}\chi H[ikU - \partial_r W + \lambda_2(ikU + \partial_r W)], \tag{A12}$$

$$\sigma \hat{M}_\varphi = -\frac{1}{\tau}\hat{M}_\varphi - (1+\lambda_2)\frac{B_{\mathrm{CCF}}}{r^2}\hat{M}_r - v_{\mathrm{CCF}}\frac{im}{r}\hat{M}_\varphi + \frac{1}{2}\chi H\left[ikV - \frac{im}{r}W + \lambda_2\left(ikV + \frac{im}{r}W\right)\right], \tag{A13}$$

$$\sigma \hat{M}_z = -\frac{1}{\tau}\hat{M}_z - v_{\mathrm{CCF}}\frac{im}{r}\hat{M}_z + \lambda_2 \chi H ikW. \tag{A14}$$

The subset of equations for the flow amplitudes contains second-order derivatives with respect to r. It is written as a system of first-order equations

$$\partial_r U = -\frac{1}{r}U - \frac{im}{r}V - ikW, \tag{A15a}$$

$$\partial_r V = \frac{im}{r}U - \frac{1}{r}V + Y, \tag{A15b}$$

$$\partial_r W = ikU + Z + (1 + \chi - \chi\lambda_2)H\hat{M}_r, \tag{A15c}$$

$$\partial_r P = -\left(\sigma + v_{CCF}\frac{im}{r}\right)U + \frac{2v_{\mathrm{CCF}}}{r}V - \frac{im}{r}Y - ikZ - ik(1-\lambda_2)\chi H\hat{M}_r, \tag{A15d}$$

$$\partial_r Y = 2A_{\mathrm{CCF}}U + \left(\sigma + v_{\mathrm{CCF}}\frac{im}{r}\right)V + \frac{im}{r}P - ikX + ik(1-\lambda_2)\chi H\hat{M}_\varphi, \tag{A15e}$$

$$\partial_r Z = \left(\sigma + v_{\mathrm{CCF}}\frac{im}{r}\right)W + ikP - \frac{1}{r}Z + \frac{im}{r}X + ik(1-\lambda_2)\chi H\hat{M}_z, \tag{A15f}$$

with

$$X = ikV - \frac{im}{r}W + [1 + \chi(1-\lambda_2)]H\hat{M}_\varphi. \tag{A15g}$$

The equations for the magnetization modes are transformed into linear algebraic equations that contain the flow modes U, V, W, Z in the inhomogeneities

$$\left[\tilde{\sigma} + \frac{1}{2}(1 - \lambda_2)\chi(1 + \chi - \chi\lambda_2)H^2\right]\hat{M}_r - (1 - \lambda_2)\frac{B_{\mathrm{CCF}}}{r^2}\hat{M}_\varphi + \frac{v_{\mathrm{CCF}}}{2}\frac{im}{r}\hat{M}_z = \left[ik\lambda_2 U - \frac{1}{2}(1 - \lambda_2)Z\right]\chi H, \tag{A16a}$$

$$(1 + \lambda_2)\frac{B_{\mathrm{CCF}}}{r^2}\hat{M}_r + \tilde{\sigma}\hat{M}_\varphi = \left[\frac{1}{2}(1 + \lambda_2)ikV - \frac{1}{2}(1 - \lambda_2)\frac{im}{r}W\right]\chi H, \tag{A16b}$$

$$\tilde{\sigma}\hat{M}_z = \lambda_2 ikW\chi H. \tag{A16c}$$

Here we have used the abbreviation

$$\tilde{\sigma} = \sigma + \frac{1}{\tau} + v_{\mathrm{CCF}}\frac{im}{r}. \tag{A16d}$$

The solution $\hat{M}_\varphi, \hat{M}_r, \hat{M}_z$ of the algebraic equations (A16) is inserted into Eqs. (A15). Then the first-order differential equations (A15) are solved by a shooting method subject to the boundary conditions $U = V = W = 0$ at the cylinders r_1 and r_2. The space of parameters that we explore is spanned by λ_2, H, m, k, Re_1, and Re_2. The two Reynolds numbers enter via A_{CCF}, B_{CCF}, and v_{CCF}, i.e., via the basic CCF state.

Here we restrict ourselves to marginal solutions with vanishing growth rate by imposing $\gamma = 0$ on the complex eigenvalue $\sigma = \gamma + i\omega$.

---

[1] R. E. Rosensweig, *Ferrohydrodynamics* (Cambridge University Press, Cambridge, 1985).

[2] B. M. Berkovsky, V. F. Medvedev, and M. S. Krakov, *Magnetic Fluids: Engineering Applications* (Oxford University Press, Oxford, 1993).

[3] B. M. Berkovsky and V. Bashtovoy, *Magnetic Fluids and Applications Handbook* (Begell House, New York, 1996).

[4] E. Blums, A. Cebers, and M. M. Maiorov, *Magnetic Fluids* (de Gruyter, Berlin, 1997).

[5] S. Odenbach, *Magnetoviscous Effects in Ferrofluids*, Lecture Notes in Physics Monograph, 71 (Springer, Berlin, 2002).

[6] R. E. Rosensweig, R. Kaiser, and G. Miskolczy, J. Colloid Interface Sci. **29**, 680 (1969).

[7] J. P. McTague, J. Chem. Phys. **51**, 133 (1969).

[8] W. F. Hall and S. N. Busenberg, J. Chem. Phys. **51**, 137 (1969).

[9] M. I. Shliomis, Sov. Phys. JETP **34**, 1291 (1972).

[10] A. N. Vislovich, V. A. Novikov, and A. K. Sinitsyn, J. Appl. Mech. Tech. Phys. **27**, 72 (1986).

[11] M. Niklas, Z. Phys. B **68**, 493 (1987).

[12] P. J. Stiles, M. Kagan, and J. B. Hubbard, J. Colloid Interface Sci. **120**, 430 (1987).

[13] M. Niklas, H. Müller-Krumbhaar, and M. Lücke, J. Magn. Magn. Mater. **81**, 29 (1989).

[14] J. Singh and R. Bajaj, J. Magn. Magn. Mater. **294**, 53 (2005).

[15] S. Altmeyer, C. Hoffmann, A. Leschhorn, and M. Lücke, Phys. Rev. E **82**, 016321 (2010).

[16] A. Leschhorn, M. Lücke, C. Hoffmann, and S. Altmeyer, Phys. Rev. E **79**, 036308 (2009).

[17] O. Ambacher, S. Odenbach, and K. Stierstadt, Z. Phys. B **86**, 29 (1992).

[18] M. A. Martsenyuk, Y. L. Raikher, and M. I. Shliomis, Sov. Phys. JETP **38**, 413 (1974).

[19] M. I. Shliomis, Phys. Rev. E **64**, 063501 (2001).

[20] P. J. W. Debye, *Polar Molecules* (Dover, New York, 1929).

[21] H. W. Müller and M. Liu, Phys. Rev. E **64**, 061405 (2001); O. Müller, D. Hahn, and M. Liu, J. Phys.: Condens. Matter **18**, S2623 (2006).

[22] S. Odenbach and H. W. Müller, Phys. Rev. Lett. **89**, 037202 (2002); J. Magn. Magn. Mater. **289**, 242 (2005).

[23] D. L. Harris and W. D. Reid, J. Fluid Mech. **20**, 95 (1964).

[24] E. R. Krueger, A. Gross, and R. C. DiPrima, J. Fluid Mech. **24**, 521 (1966).

[25] J. Embs, H. W. Müller, C. E. Krill III, F. Meyer, H. Natter, B. Müller, S. Wiegand, M. Lücke, R. Hempelmann, and K. Knorr, Magnetohydrodynamics **37**, 222 (2001).

[26] A. Leschhorn and M. Lücke, Z. Phys. Chem. **220**, 89 (2006).

[27] J. P. Embs, S. May, C. Wagner, A. V. Kityk, A. Leschhorn, and M. Lücke, Phys. Rev. E **73**, 036302 (2006).

[28] A. Leschhorn, J. P. Embs, and M. Lücke, J. Phys.: Condens. Matter **18**, 2633 (2006).

[29] J. Embs, H. W. Müller, M. Lücke, and K. Knorr, Magnetohydrodynamics **36**, 387 (2000).

[30] J. Embs, H. W. Müller, C. Wagner, K. Knorr, and M. Lücke, Phys. Rev. E **61**, R2196 (2000).

[31] M. Reindl and S. Odenbach, Phys. Fluids **23**, 093102 (2011).

[32] M. Reindl and S. Odenbach, Exp. Fluids **50**, 375 (2010).